New Anderson-Based Polyoxometalate Covalent Organic Frameworks as Electrodes for Energy Storage Boosted Through Keto-Enol Tautomerization

Dawid Pakulski, Adam Gorczyński, Daria Brykczyńska, Verónica Montes Garcia, Wlodzimierz Czepa, Iwona Janica, Michal Bielejewski, Maciej Kubicki, Violetta Patroniak, Paolo Samorì, et al.

How to cite: *Angew. Chem. Int. Ed.* **2023**, *62*, e202305239
doi.org/10.1002/anie.202305239

Supercapacitors | Very Important Paper

New Anderson-Based Polyoxometalate Covalent Organic Frameworks as Electrodes for Energy Storage Boosted Through Keto-Enol Tautomerization

Dawid Pakulski, Adam Gorczyński, Daria Brykczyńska, Verónica Montes-García, Włodzimierz Czepa, Iwona Janica, Michał Bielejewski, Maciej Kubicki, Violetta Patroniak, Paolo Samorì,* and Artur Ciesielski**

Abstract: The unique electrochemical properties of polyoxometalates (POMs) render them ideal components for the fabrication of next-generation high-performance energy storage systems. However, their practical applications have been hindered by their high solubility in common electrolytes. This problem can be overcome by the effective hybridization of POMs with other materials. Here we present the design and synthesis of two novel polyoxometalate-covalent organic frameworks (POCOF) via one-pot solvothermal strategy between an amino-functionalized Anderson-type POM and a trialdehyde-based building unit. We show that structural and functional complexity can be enriched by adding hydroxyl groups in the 2,4,6 position to the benzene-1,3,5-tricarbaldehyde allowing to exploit for the first time in POCOFs the keto-enol tautomerization as additional feature to impart greater chemical stability to the COFs and enhanced properties leading to large specific surface area (347 m^2/g) and superior electrochemical performance of the POCOF-1 electrodes, when compared with POCOF-2 electrodes that possess only imine-type linkage and with pristine POM electrodes. Specifically, POCOF-1 electrodes display remarkable specific, areal, and volumetric capacitance (125 F/g, 248 mF/cm^2 and 41.9 mF/cm^3, respectively) at a current density of 0.5 A/g, a maximum energy density (56.2 Wh/kg), a maximum power density (3.7 kW/kg) and an outstanding cyclability (90 % capacitance retention after 5000 cycles).

Introduction

Energy supply for on-demand utilization has become one of the most urgent global challenges due to the transition to sustainable and clean energy sources alternative to fossil fuels. An enormous research effort is nowadays devoted to the fabrication of novel high-performance energy storage systems (ESS), including capacitors, supercapacitors (SCs) (such as electrical double layer capacitors (EDLC) and pseudocapacitors), batteries and hybrid systems.[1] While capacitors and EDLC SCs are most suitable for applications requiring a quick burst of energy as they can achieve high power densities (10–20 kW/kg), fast charge/discharge time (1–10 s), and long lifespan ($>10^5$ cycles),[2] batteries are more apt for long-term energy needs due to their high energy densities (100–200 Wh/kg).[3] Pseudocapacitors and hybrid ESS represent a viable strategy to obtain devices with high energy and power density.[4] On the one hand, pseudocapacitors store charges based on Faradaic redox reactions on the surface or near the surface of the electrode active materials, without ion diffusion within the bulk of the electrode active materials. On the other hand, hybrid ESS exhibit a behavior intermediate between EDLC and Faradaic processes. Such a combination is typically accomplished at the device level, by exploiting architectures comprising one battery-type electrode and one capacitive electrode. A key step forward could be achieved by attaining such a hybridization at a material level, through the

[*] Dr. D. Pakulski
Adam Mickiewicz University Foundation, Poznań Science and Technology Park
Rubież 46, 61-612 Poznań (Poland)
E-mail: dawid.pakulski@amu.edu.pl
Dr. D. Pakulski, Dr. A. Ciesielski
Centre for Advanced Technologies, Adam Mickiewicz University
Uniwersytetu Poznańskiego 10, 61-614 Poznań (Poland)
Dr. A. Gorczyński, D. Brykczyńska, W. Czepa, Dr. I. Janica, Prof. M. Kubicki, Prof. V. Patroniak
Faculty of Chemistry, Adam Mickiewicz University
Uniwersytetu Poznańskiego 8, 61-614 Poznań (Poland)
Dr. V. Montes-García, Prof. P. Samorì, Dr. A. Ciesielski
Université de Strasbourg, CNRS, Institut de Science et d'Ingénierie Supramoléculaires
8 allée Gaspard Monge, 67000 Strasbourg (France)
E-mail: samori@unistra.fr
ciesielski@unistra.fr
Dr. M. Bielejewski
Institute of Molecular Physics, Polish Academy of Sciences
M. Smoluchowskiego 17, 60-179 Poznań (Poland)

development of materials capable to accomplish both types of charge storage mechanisms. Although this process has been pursued by blending of different materials, the engineering of hybrids capable to express both storage mechanisms has been barely explored or incorrectly classified.[5] Therefore, the development of novel nanostructured electrode materials with improved electrochemical performance is key for the next generation of ESS. In general, the nature of the charge storage (pseudocapacitive or hybrid) cannot be easily predicted a priori. Among various characteristics that need to be optimized in the material's engineering, the surface area, porosity, conductivity and electrochemical activity have been identified as the fundamental properties that strongly influence the electrochemical performance of electrodes in ESS.[6] In particular, electrode materials with electrochemically-active groups usually exhibit considerably larger specific capacitances/capacities compared with EDLC SCs.[7]

Polyoxometalates (POMs) represent a well-established family of anionic metal oxide clusters, which can be defined as isopoly- or heteropolyanions depending on the presence of only one metallic element M.[8] As a result of their structural and functional diversity, POMs have been successfully used in myriad applications,[8a,9] including electro- and photo-catalysis,[10] antiviral agents,[11] and as EES systems.[12] Importantly, thanks to their unique electrochemical properties and ability to act as electron reservoirs, POMs are the ideal candidates for the fabrication of novel high-performance ESS. Although POMs electrodes have shown a high stability of their redox states and can participate in fast reversible multielectron-transfer reactions, their high solubility in water and many organic solvents makes them unsuitable for many practical applications.[12a] Fortunately, this problem can be overcome through the hybridization of POMs with other materials.[13] Nanostructured carbon-based materials including activated carbon, carbon nanotubes, and graphene have been widely used as POM supports to enhance their stability, large surface areas, and high electronic conductivity.[14] Nevertheless, the carbonaceous materials typically investigated are predominantly derived from finite resources like coal or graphite, indicating the need for alternative materials to be considered. Metal organic frameworks (MOFs)[15] and covalent organic frameworks (COFs)[16] constitute a rapidly growing class of crystalline organic polymeric materials, which exhibit numerous features highly desirable for EES systems, including the tuneability of their well-defined chemical structures, extraordinary thermal and chemical stabilities, high porosity, and large internal surface areas. In order to take advantage of such characteristics, POM-MOF (POMOF)[17] and POM-COF (POCOF) hybrids have been developed. While POMOFs are been the subject of various studies,[13b,18] the design, synthesis and application of POCOFs are still in their infancy. Based on their all-covalent nature, the chemical stability of POCOFs is expected to be higher than POMOFs and thus a higher electrochemical performance can be foreseen. At present, only five POCOFs have been fabricated, all via the Schiff-base condensation of diamino H_2N-POM-NH_2 and different tetraaldehydes.[19]

In their seminal work in 2012, Banerjee and co-workers reported the first example of a reaction sequence, proposing a method for the synthesis of ß-ketoenamine-linked COFs. By reacting linear diamine linkers, such as 1,4- phenylenediamine, with the hydroxylated reagent 1,3,5-triformylphloroglucinol as tritopic knot in place of the geometrically equivalent 1,3,5-triformylbenzene, the authors observed the formation of the new linkage.[20] The reaction started with the aldehyde-amine reversible condensation according to the Schiff base reaction, promoting the formation of a long-range ordered structure. Subsequently, a quantitative irreversible proton tautomerization ensured the locking of the carbon-nitrogen bond switching from the enol-imine to the keto-enamine form. Although ß-ketoenamine-linked COFs have been widely studied due to their superior chemical stability, to the best of our knowledge, this strategy has never been employed for POCOF synthesis. It is worth noting that the main application of POCOFs has been as catalysts,[19b–d] and only two POCOFs have been explored for energy-related applications. In particular, Yaghi et al.[19a] synthesized a novel POCOF and used it as a solid-state electrolyte in the prototype lithium metal battery owing to its exceptional ionic conductivity (3.4×10^{-4} S cm^{-1} at 20 °C). Li and Fang studied the Mn-Anderson-type based POCOF system as anode material for lithium-ion batteries, which showed remarkable capacity, rate capability and cycling stability.[19e] To the best of our knowledge, the electrochemical performance of POCOFs as cathodes has never been explored.

Herein, we present the synthesis of two novel POCOF based on the condensation of an amino-functionalized POM with a trialdehyde-based building unit. Two different aldehyde-based monomers, which differ by the presence/absence of hydroxyl groups in the 2,4,6 position in the benzene-1,3,5-tricarbaldehyde scaffold, are employed, resulting in formation of POCOF-1 and POCOF-2 materials, respectively. Typically, when hydroxyl groups are located next to the aldehyde moieties within one of the building units, tautomerization from the enol-imine to the keto-enamine form occurs in imine-linked COFs.[20] While the crystallinity and pore properties of the COFs are maintained, the partial transformation of imine to a ß-ketoenamine ensures a higher chemical stability and therefore is highly sought-after. We reveal for the first time the coexistence of imine/phenol and ß-ketoenamine forms in POCOF-1 by means of solid state nuclear magnetic resonance (ssNMR) and X-ray photoelectron spectroscopy (XPS) analyses together with ^{1}H NMR and ^{13}C NMR analyses of the model compounds (i.e., by using mono-aldehydes building units). To demonstrate the superior chemical stability and electrochemical performance of POCOF-1 with respect to POCOF-2 and the pristine POM, a symmetric cell with our materials acting as electrodes and 1-ethyl-3-methylimidazolium chloride (EMIMCl) ionic liquid electrolyte is assembled. POCOF-1 electrodes exhibited a superior performance (i.e., specific capacitance of 125 F/g) compared to other POM-based electrodes as well as an outstanding cyclability (90 % capacitance retention after 5000 cycles). Significantly, POCOF-1 hybrid-based electrodes also dis-

played both high energy and power density (56.2 Wh/kg and 3.7 kW/kg, respectively), comparable to lithium-ion batteries.

Results and Discussion

Synthesis and structural characterization

Anderson-type polyoxometalates $[H_y(XO_6)M_6O_{18}]^{n-}$ (y = 0–6, n = 2–8, M = addend atom, X = heteroatom) are among the most important group of the POM family as a result of their straightforward synthesis.[21] We synthesized pristine Anderson-type POM functionalized with TRIS (tris(hydroxymethyl)aminomethane), $(H_2N\text{-}(CoMo_6)\text{-}NH_2)$ by using a modified reported procedure by Schönweiz (see Experimental Section for details and Figures S1, S2).[22] Each POM contains two amino groups which serve as anchoring points for the POCOF synthesis via condensation with aldehyde-based building units. Two different aldehydes, namely benzene-1,3,5-tricarbaldehyde (BTC) and 2,4,6-triformylphloroglucinol (TFP), have been selected as precursors in this study to evaluate the effect of appended OH groups on the electrochemical performance of the obtained hybrid electrodes. The POCOFs synthesis has been accomplished by a conventional solvothermal strategy as illustrated in Figure 1. A condensation between Anderson-type POM with TFP or BTC was performed in 3:2 molar ratio to account for the exhaustive imine bond formation as the linkage. Specifically, the system was heated at 80 °C for three days in the dimethylformamide (DMF) in the presence of trifluoroacetic acid, which is responsible for pH control.

To demonstrate that the increased porosity of newly generated POCOFs con determine an improvement in the performance of materials in energy-related applications, discrete model compounds, i.e., POCOF-1 and POCOF-2 precursors have been constructed from the same Anderson-type POM and the mono-aldehydes building units (Figures S3–S8). The insolubility of POCOFs render them inadequate for ^{1}HNMR and ^{13}CNMR analyses in solution. Therefore, in order to get in-depth insight into the type of linkage present in each POCOF, which we anticipate can have a strong influence on the electrochemical performance and the cycling stability, the studies were carried out also on the POCOF precursors. POCOF-1 and POCOF-2 precursors have been obtained by heating respective substrates for two days (see experimental section for details)[19c] and were purified via crystallization. The use of these conditions in the POCOFs and POCOF precursors synthesis guarantee the imine/enamine bond formation and the POM stability.[23] Importantly, for POCOF-1 and POCOF-1 precursor, the ß-keto-enamine/phenol-imine equilibrium can be envisaged,[24]

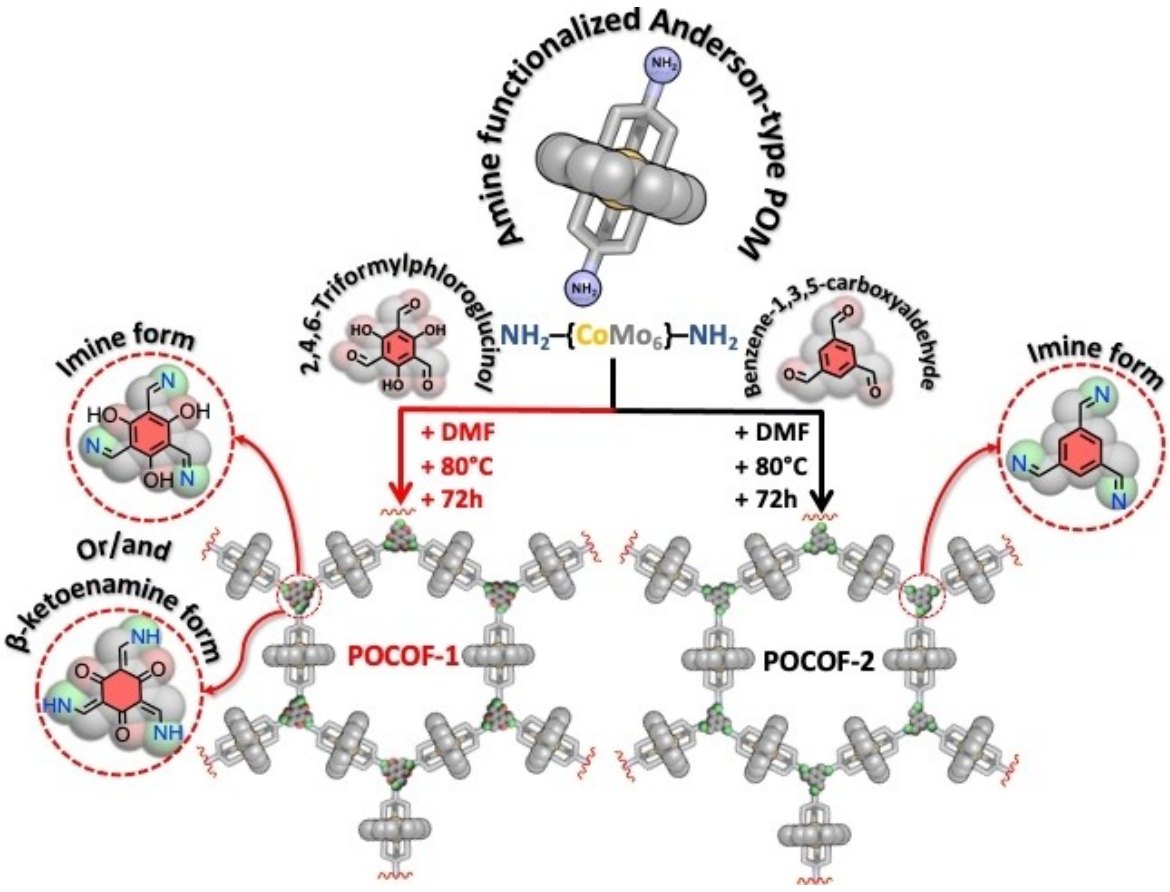

Figure 1. Synthetic pathway of POCOF-1 and POCOF-2.

whereas only the imine form can be predicted for the POCOF-2 and POCOF-2 precursor materials.

Fourier transform infrared spectroscopy (FTIR) spectra (Figure 2a) provided evidence for the successful formation of the POCOFs. Both POCOFs (Figure 2a, red and black spectra), showed the absence of the N–H stretching vibration of the pristine Anderson-type POM (~2900 cm^{-1}) (Figure 2a, blue spectrum). The aldehyde C=O stretching vibration of the building units (1658 cm^{-1} and 1687 cm^{-1} for TFP[25] and BTC[26] respectively, Figure S9) was shifted towards lower wavenumbers (1627 cm^{-1} and 1631 cm^{-1} for POCOF-1 and POCOF-2, respectively) and can be ascribed to C=N imine or to a new C=O stretching vibration (i.e., in the case of ß-ketoenamine form). Signals at 1253 cm^{-1} and 1254 cm^{-1} for POCOF-1 and POCOF-2, respectively, can be attributed to C–N stretching vibration. This signal originates from the C–N present in the TRIS part of the Anderson-POM as well as from the C–N bond in the case of ß-ketoenamine form. As can be seen in the Figure 2a, the relative intensity of this signal is higher in POCOF-1, giving the first sign of the co-existence of imine/phenol and ß-ketoenamine forms in POCOF-1. An analogous behavior was observed for the POCOF precursors (Figure S10). The stretching vibrations ascribed to the pristine POM at ~650 cm^{-1} and ~900 cm^{-1}, are present in the POCOF and POCOF precursor materials, confirming the stability of the POM during the synthetic procedure. Finally, an extensive network of hydrogen bonding was observed for POCOF-1 between the 3500–2000 cm^{-1} region, resulting from both imine/phenol and ß-ketoenamine forms. FTIR spectra also show (Figure S10) the disappearance of the NH signals (range 3500–3300 cm^{-1}) from the pristine POM in POCOF-2 precursor, whereas they are shifted in POCOF-1 precursor, indicating the presence of the keto/enol equilibrium.

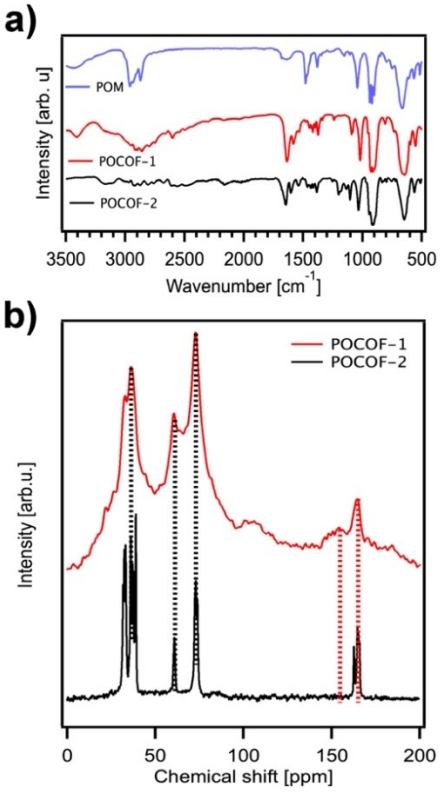

Figure 2. a) FTIR spectra of H_2N-($CoMo_6$)-NH_2 Anderson POM, POCOF-1 and POCOF-2 b) C^{13} solid state NMR spectra of POCOF-1 and POCOF-2.

To gain insight into the presence of imine, imine/phenol or ß-ketoenamine forms in the POCOFs and POCOF precursors and further confirm the successful syntheses, cross-polarization magic angle spinning (CP/MAS) solid state ^{13}CNMR (Figure 2b and S11) has been then performed. Contrary to POCOF-1, whose signals are significantly broad as a result of the hydrogen bonding between carbonyl and amine groups, POCOF-2 exhibited very sharp signals. The same behavior was observed for the POCOF precursors, although the hydrogen bonding is weaker in POCOF-1 precursor (isolated molecules) compared to the POCOF-1 (3D polymeric material). The signals ascribed to imine and enamine can be observed in the range from 150 to 180 ppm. While POCOF-2 and POCOF-2 precursors exhibited only one sharp signal, confirming the presence of imine-linkage exclusively, two signals can be observed for POCOF-1 precursor and for POCOF-1 (dashed red lines), revealing the co-existence of imine and enamine-linkage.

To unambiguously confirm the nature of linkages in the POCOF precursors, single crystal X-ray diffraction measurements and difference Fourier maps have been performed (see Table S1, Figure S12–13). Difference Fourier maps of POCOF-1 precursor, calculated without the O/N hydrogen atoms (Figure S12) clearly showed that the crystal structure contains a mixture of OH and NH forms. Additionally, to further confirm the presence of ß-ketoenamine form in POCOF-1 and POCOF-1 precursor, solution state ^{1}HNMR and ^{13}CNMR spectra have been recorded for both precursors in d_6-DMSO and d_3-MeCN (Figures S3–S8). The ^{1}HNMR of POCOF-1 precursor revealed predominant signals of the imine form when DMSO is used as solvent and the co-existence of the signals of ß-ketoenamine and imine form when CD_3CN is employed. To observe the ß-ketoenamine form in solution a solvent with high polarity is needed (0.444 (DMSO) vs. 0.46 (MeCN) when hexane/H_2O scale is used). The second factor that can shift the equilibrium between the imine/phenol and ß-ketoenamine forms is the occurrence of hydrogen bonding with the solvent (i.e., phenolic proton can dissociate easier from phenol than from NH). In d_6-DMSO the hydrogen bond interactions with the imine/phenol form are stronger than in d_3-MeCN and therefore the equilibrium is shifted towards the imine/phenol form in DMSO and both imine/phenol and ketoenamine forms are present in MeCN.[27] Moreover, the ^{13}CNMR spectrum of POCOF-1 precursor revealed a signal at 199 ppm, corresponding to the C=O of the ß-ketoenamine form (Figure S5). The ^{1}HNMR spectrum of POCOF-2 precursor, as expected, exhibited the signals of imine form in both solvents. However, in d_3-MeCN, the signals corresponding to the aldehyde building unit were also observed, indicating the lower chemical stability of POCOF-2 (Figures S6–8, S14). By comparing the ratio of aromatic integrated

signals from POCOF-2 precursor and from the hydrolyzed aldehyde, the decomposition yield to the corresponding benzaldehyde and H_2N-$CoMo_6$-NH_2 POM can be quantified as ca. 20 % in d_3-MeCN and 3 % in d_6-DMSO.

To gain deeper insight into chemical composition of POCOFs, X-ray photoelectron spectroscopy (XPS) analyses have been carried out (Figures 3 and S15, S16). Figure S15 shows the survey of POM, POCOF-1 and POCOF-2 revealing the presence of C, N, O, Mo, Co elements in all three cases. The main differences between pristine POM and POCOFs can be observed in the high-resolution spectra of C1s and N1s (Figure 3).

The analysis of C1s spectra of POCOF-1 and POCOF-2 revealed three peaks at 284.8, 286.4 and 287.9 eV, corresponding to the chemical bonds based on carbon-carbon (C–C and C=C), carbon-heteroatom (C–O and C–N) and C=N, respectively. The N1s spectrum of pristine POM provided evidence for the existence of features at 397.8 and 402 eV, which can be assigned to primary and quaternary amines, respectively. On the other hand, N1s spectra of POCOF-1 and POCOF-2 revealed the existence of peak at 401.7 eV corresponding to the chemical bond C=N, thereby indicating the formation of imine bonds. Noteworthy, in POCOF-1 we can also clearly observe an additional peak at 399.7 eV due to C–N–C enamine bond. The Mo_{3d} high-resolution spectra confirms that the POM remains stable during the formation of POCOFs as no reduction of Mo^{6+} centers to Mo^{5+} centers occurs (Figure S16).[28] In addition, the positive shift in the Mo 3d binding energy accounts for the electron transfer on chemical bonding associated with formation of hybrid COF materials.[19d]

Ultimately, the POCOFs synthesis can be divided in two steps: initially, a reversible Schiff base reaction leads to the formation of a crystalline framework, and subsequently an irreversible enol-to-keto tautomerization takes place, which enhances the chemical stability of the system.[20] While for POCOF-2 only the first step takes place, for POCOF-1 the second step can also occur due to the presence of hydroxyl groups. Altogether, FTIR, solid state ^{13}CNMR, solution state ^{1}HNMR and ^{13}CNMR and XPS provide unambiguous evidence that for POCOF-1 a mixture of imine/phenol and ß-ketoenamine forms is obtained (Figure S17), which differs from the complete tautomerization phenomenon observed for COF frameworks.[29] The incomplete tautomerization can be a result of high negative charge of the POM counterpart (zeta potential of -38.5 ± 0.59 mV), thus generating an electrostatic repulsion between POM units and interacting with the tautomerizable hydrogen through the

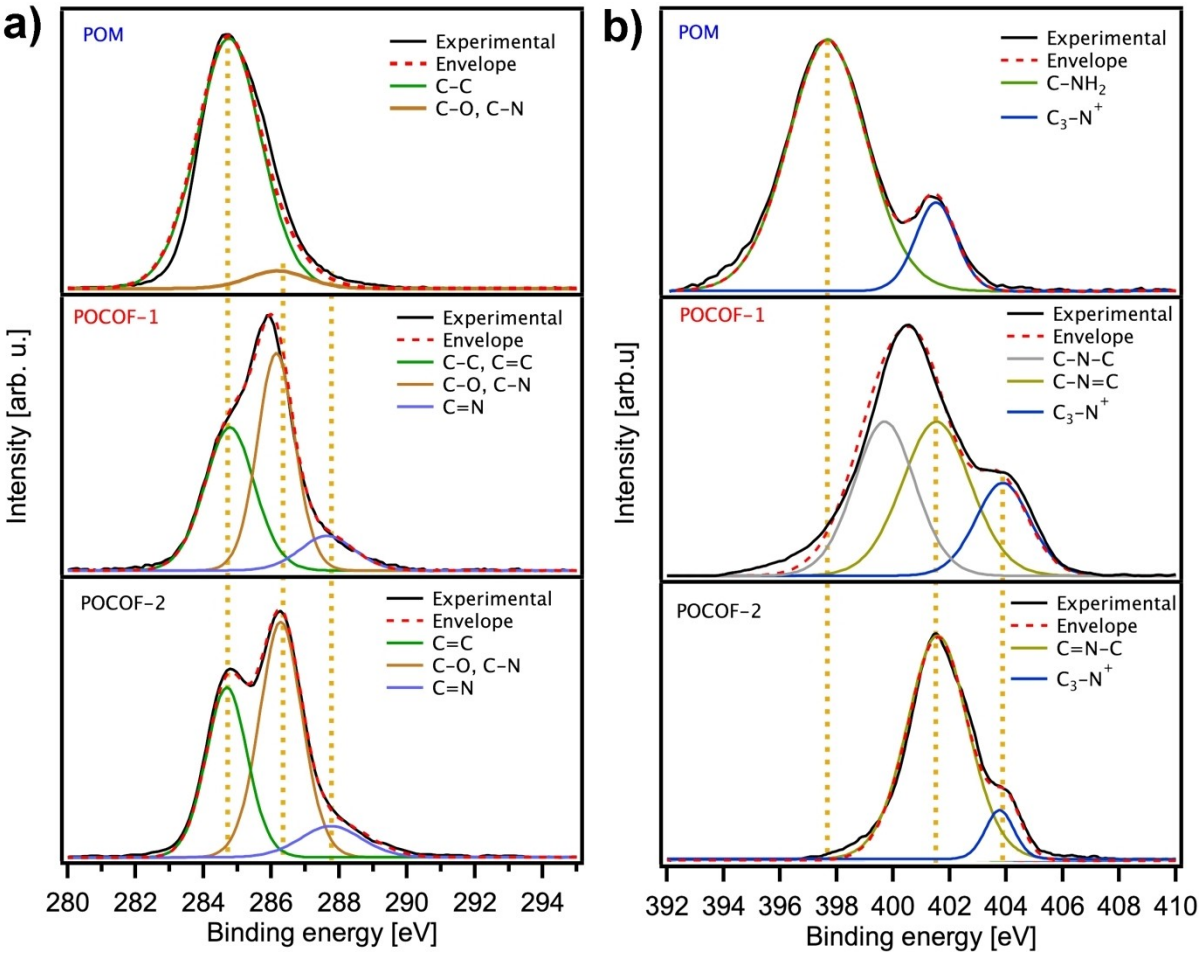

Figure 3. a) C1s and b) N1s XPS analysis of POM, POCOF-1 and POCOF-2.

molybdenum-oxo clusters, ultimately shifting the equilibrium towards imine/phenol form.

Scanning electron microscopy (SEM) images revealed the morphology and microstructure of the as-prepared POM and POCOFs materials (Figure 4a–c). While pristine POMs are assembled into elongated crystals, the POCOF-2 morphology resemble a cauliflower. Strikingly, the presence of OH groups at the benzene moiety in POCOF-1 determines a completely different morphology.

The porosity of POM, POCOF-1 and POCOF-2 has been evaluated by acquiring nitrogen adsorption-desorption isotherms at 77 K (Figure 44d). The adsorption isotherms exhibited Type-IV sorption features in the three cases, indicating a microporous nature for most pores with typical sizes of 1.7, 1.8 and 2.5 nm for POM, POCOF-1 and POCOF-2, respectively, calculated with the Barrett-Joyner-Haleda (BJH) model (Figure S18). The calculated Brunauer–Emmett–Teller (BET) surface areas of POCOF-1 and POCOF-2 amounted to 347 m^2/g and 176 m^2/g, respectively, being ca. 8 and 4 times greater than the specific surface area of the pristine POM (43 m^2/g, Figure 4d), and significantly higher than recently reported POCOF materials.[19c] For instance, Zhang et al. exploited a covalent bond-driven strategy to obtain polyoxometalate based open frameworks using planar tetra-aldehyde monomers, exhibiting a surface area of 134 m^2/g.[19c]

Powder X-ray diffraction (PXRD) patterns of POM, POCOF-1 and POCOF-2 are portrayed in Figure 4d. Pristine POM exhibits a sharp peak at $2\theta = 8.7°$ which corresponds to the 001 plane. The two POCOFs display PXRD patterns that are typical of 2D layered hexagonal networks.[25] The main peak of the pristine POM is slightly shifted in both POCOFs (8.5°) together with the simultaneous appearance of new peaks at 7.4° for POCOF-1 and 6.7 and 13.5° for POCOF-2. Pristine COFs commonly exhibit the 001 plane at $2\theta < 5°$, which translates in small interplanar distances (i.e., $d < 1.77$ nm) and additional stabilization interactions, mostly non-covalent (e.g., π–π stacking). In full agreement with the PXRD of other POCOFs,[19a–d] the size and negative charge of the POM counterpart results in a 001 plane at $2\theta > 5°$. It is important to highlight that in the case of POCOF-1, the irreversible nature of the tautomerism does not affect the crystallinity of the POCOF, since the transformation involves only shifting of bonds while keeping the atomic positions almost constant.[20]

Thermal stability of POM and POCOFs materials has been assessed by using thermogravimetric analysis (TGA) (Figure S19). The superior thermal stability of the POCOF-1 material is confirmed when compared with POCOF-2 due to the presence of the covalently-linked ß-ketoenamine. Specifically, the thermal decomposition of POCOF-1 starts from 160 °C, whereas the linear degradation of POCOF-2 is observed from 60 °C on.

The electrochemical performance of all POCOFs electrodes as well as pristine POM electrode has been assessed in a symmetrical two-electrode configuration by using 1-ethyl-3-methylimidazolium chloride (EMIMCl) ionic liquid as electrolyte. The use of EMIMCl as electrolytes has several advantages including high chemical, thermal and

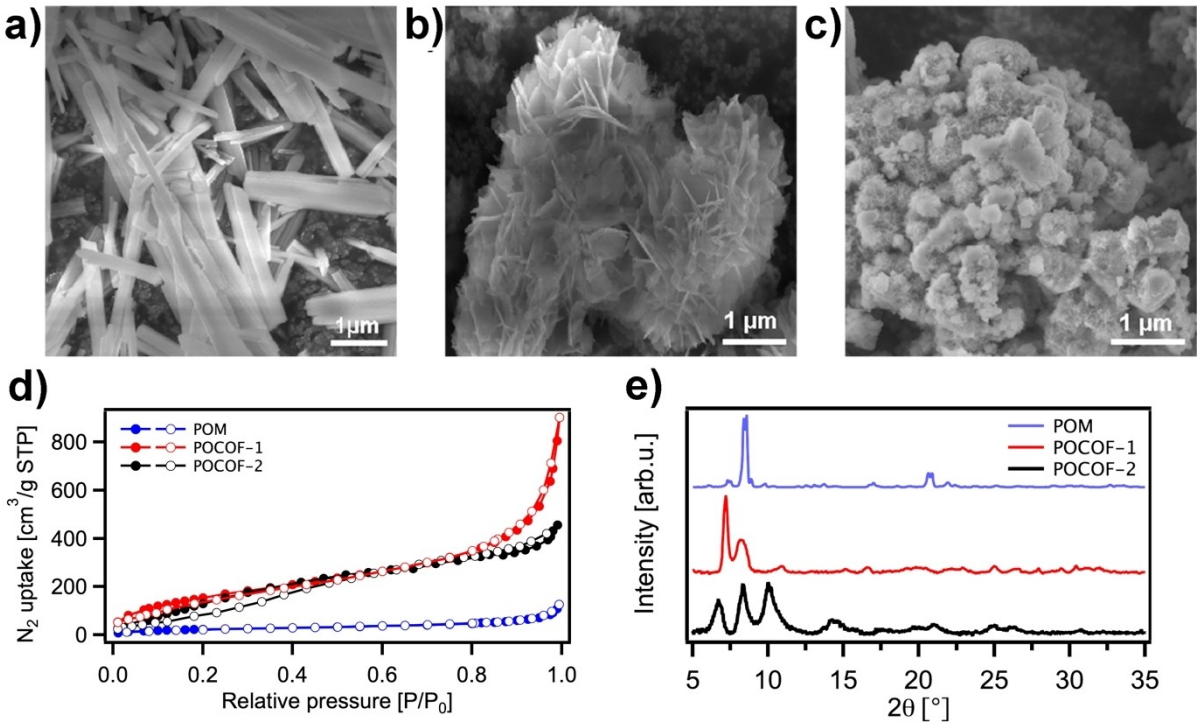

Figure 4. SEM images of a) POM, b) POCOF-1 and c) POCOF-2. d) BET surface area of POM, POCOF-1 and POCOF-2. e) PXRD of POM, POCOF-1 and POCOF-2.

electrochemical stability, negligible volatility, non-flammability and stability in a broad potential window.[30] Figure 5a–b and Figure S20a display cyclic voltammetry (CV) curves of (S20a) POM, (5a) POCOF-1 and (5b) POCOF-2 between 0 and 1.8 V at scan rates from 2 to 1000 mV/s. Although ionic liquids allow to extend the potential window up to 4 V, the operating potential of the final devices depends on both, the electrolyte and the electrode material.[31] Both POCOFs and the pristine POM electrodes exhibited a good rate capability up to a scan rate of 1000 mV/s, evidenced by the maintained box-like shapes of their CVs.

The kinetics of electrochemical processes occurring at POM, POCOF-1 and −2 electrodes have been investigated by exploiting the procedure proposed by Wu et al.,[32] according to the equation: $i = av^b$, where i represents current density, ν refers to scan rate, a and b are variable parameters. The value of b ranges from 0.5 (battery-type materials) when the charge storage mechanism is ruled by diffusion-controlled processes, up to 1 (EDLC SCs and pseudocapacitors) when the charge storage mechanism is governed by capacitive-controlled processes or fast surface redox reactions. When b value is in-between 0.5 and 1, both diffusion and capacitive-controlled processes coexist (hybrid materials). The average value of b for POM, POCOF-1 and −2 electrodes resulted 0.64, 0.65 and 0.63, indicating that POM and both POCOFs possess a hybrid nature with a charge storage mechanism predominantly ruled by a diffusion contribution and partial capacitive contribution (Figure S21).[7b]

A possible hybrid charge storage mechanism can be as follows: electrolyte ions can coordinate the metal ions of the POM (Co and Mo) through a capacitive charge storage mechanism, as at the operating potential window Co and Mo show no redox activity. Additionally, in POCOF-1, electrolyte ions can also coordinate with the redox-active carbonyl units of the ß-ketoenamine form. To access the metal ions of the POMs, electrolyte ions have to diffuse through the POM structure via a diffusion charge storage mechanism. On the same time, electrolyte ions can also be stored in the accessible interstitial sites on the interface or pores of POCOFs or in the carbonyl units of the organic building unit of POCOF-1 through a capacitive charge storage mechanism. Figure 5c–d and Figure S20b show the galvanostatic charge/discharge (GCD) curves of (Figure S20c) POM, (Figure 5c) POCOF-1 and (Figure 5d) POCOF-2 between 0 and 1.8 V at current densities from 0.5

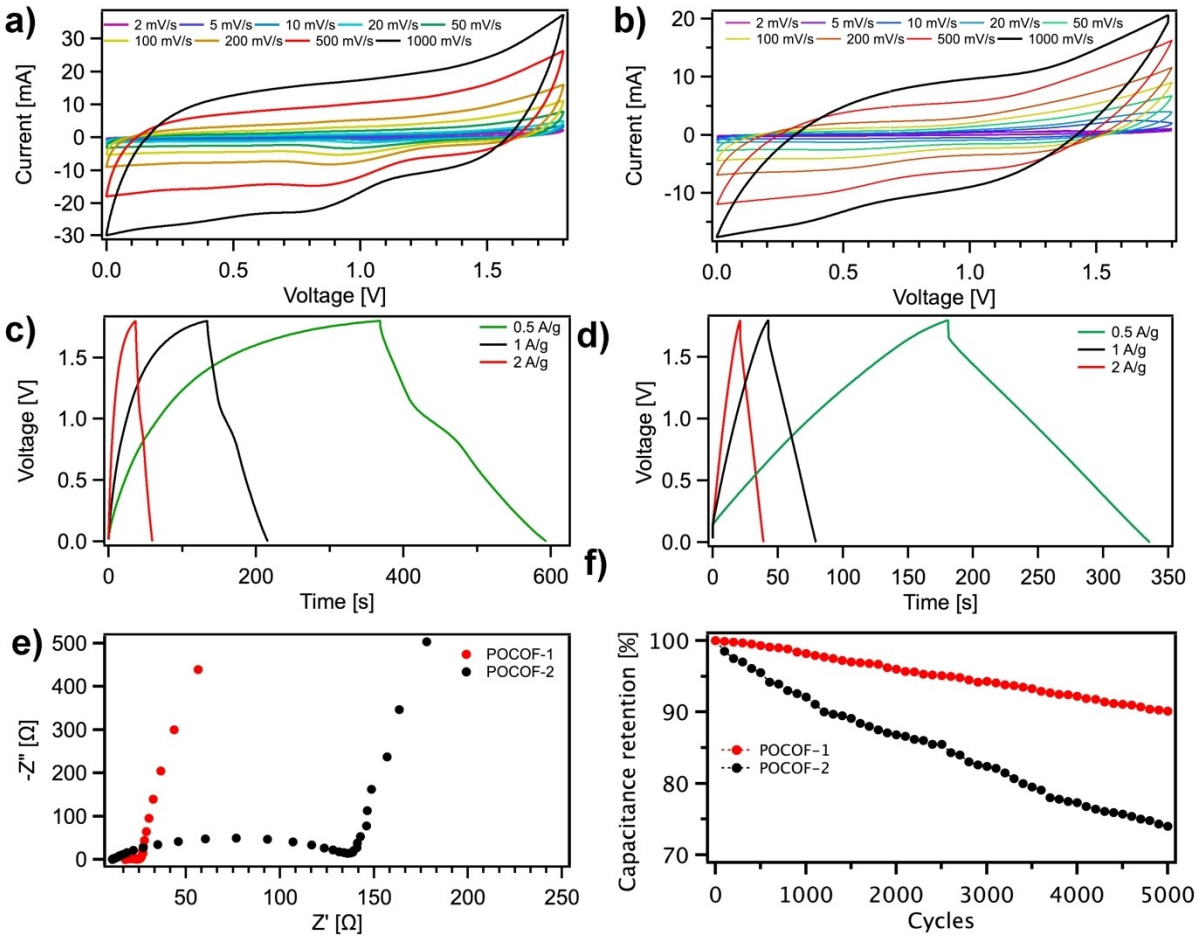

Figure 5. Electrochemical characterization of POCOF-1 and POCOF-2 in a two-electrode system configuration. CV curves at different scan rate for a) POCOF-1 and b) POCOF-2. GCD at different current densities for c) POCOF-1 and d) POCOF-2. e) Nyquist plots for POCOF-1 and POCOF-2. f) Capacitance retention upon cyclin.

to 2 A/g. In full agreement with the CV and kinetic analysis, the GCD profiles of POM, POCOF-1 and −2 displayed a non-symmetric triangular shape due to its hybrid nature. Notably, the electrochemical performance of POCOF electrodes, in terms of capacitance, resulted 3–5 times greater than the one of the pristine POM electrodes (25 F/g), the POCOF precursors electrodes (38 and 27 F/g for POCOF-1and −2 precursors, respectively), as well as other POM-based electrodes (see Table S2–5, Figure S22). Specifically, POCOF-1 electrodes exhibited a higher specific capacitance, 125 F/g, at current density of 0.5 A/g, compared to POCOF-2 electrodes, which amounts to 85 F/g at the same current density. Furthermore POCOF-1 and POCOF-2 electrode materials also revealed an outstanding areal capacitance (248 and 170 mF/cm^2, respectively) and volumetric capacitance (41.9 and 28.6 mF/cm^3, respectively) at the same current density. Remarkably, because of their hybrid nature, our POCOF-based electrodes (Table S2) displayed an outstanding maximum energy density (56.2 and 38.2 Wh/kg for POCOF-1 and POCOF-2, respectively) and power densities of (3.7 and 3.6 kW/kg, for POCOF-1 and POCOF-2 respectively), which are beyond the state of the art of all previously reported POM-hybrids, COFs, MOFs and carbon based electrode materials. The better electrochemical performance of POCOF-1 electrodes can be attributed to the higher surface area of POCOF-1 compared to POCOF-2 (347 vs 176 m^2/g), as well as to the additional contribution of the redox-active carbonyl groups in POCOF-1.[33]

Electrochemical impedance spectroscopy (EIS) data has been analyzed using Nyquist plots (Figure 5e) to shed some light on the interactions of the electrode materials with the electrolyte and with the current collector. The experimental results were well fitted with the indicated circuit (Figure S23 and Table S6). Rs depicts the combined internal resistance, including the interfacial contact resistance of the material with the current collector, the ohmic resistance of the electrolyte and the intrinsic resistance of the current collector. The magnitudes of the Rs for both POCOFs are lower than 18 Ω. The low internal resistance is consistent with the fact that at a scanning rate as high as 1000 mV/s, the CV curves still show a rectangular shape with small distortion, indicating that the POCOF samples possess a good rate capability and a good interaction with the current collector. R_{ct} is the interfacial charge transfer resistance, which represents the resistance of electrochemical reactions at the electrode surface. The magnitude of the R_{ct} amounts to 6.2 Ω and 115.3 Ω for POCOF-1 and POCOF-2, respectively. The lower R_{ct} of POCOF-1 is consistent with the absence of IR drop due to the fact that POCOF-1 possess electrochemically active groups that facilitate the interaction with the electrolyte. On the contrary, POCOF-2 exhibited an IR drop at the current densities from 0.5 to 2 A/g, suggesting a worse interaction on the electrode-electrolyte interface compared to POCOF-1.[34] This is in full agreement with the higher charge transfer resistance obtained for POCOF-2 (115.3 Ω) compared to POCOF-1 (6.2 Ω).The ionic conductivity of POM and POCOF-based electrodes is obtained by EIS (see Table S6). The ionic conductivity of both POCOFs is ~0.043 S/m, which indicates a two fold enhancement compared to the pristine POM′s ionic conductivity of 0.019 S/m. To gain a greater insight into the electrical performance of POM-based materials, electrical conductivity measurements are then performed. Pellets of the different materials are prepared (see experimental information) and the film conductivity is measured with a probe station. Among the different samples, pristine POM exhibits the lowest electrical conductivity (3.01×10^{-7} S/m), comparable to other reported POMs.[35] Interestingly, the electrical conductivity of POCOF materials amount to POCOF-1 $=3.41\times10^{-5}$ S/m and POCOF-2 $=4.59\times10^{-6}$ S/m being two and one orders of magnitude higher than the H_2N-$CoMo_6$-NH_2 polyoxometalate, respectively. The enhanced conductivity observed can be attributed to the effective integration of POM into the COF framework, leading to a more organized molecular structure and improved conductivity. The difference in conductivity between POCOF-1 and POCOF-2 can be ascribed to the nature of the starting aldehyde. While POCOF-2 exhibits only imine binding, the presence of a tautomerizable phenol/imine counterpart in POCOF-1 contributes to the polarizability of the organic scaffold and the occurrence of hydrogen bonding.

Finally, to investigate the electrochemical stability of the POM and the as-prepared POCOFs electrodes, GCD cycling has been executed at current density of 0.5 A/g (Figure S20c and Figure 5f). POCOF-1 electrodes revealed an outstanding cyclability with a capacitance decay of only ~10 % after 5000 working cycles. Differently, the capacitance decay after 5000 cycles for POCOF-2 electrodes increased up to 26 % and up to 59 % in the pristine POM electrodes. The difference in long-term stability of POCOF-1 and POCOF-2 electrodes can be ascribed to the instability of imine-linkages which are prone to hydrolysis.

Conclusion

In summary, we have demonstrated that Anderson-type polyoxometalate can be used as building block for the fabrication of new covalent organic framework hybrids (POCOFs) with enhanced performance. We have shown that the presence of appended hydroxyl groups affects not only the chemical properties of the hybrids but also their electrochemical characteristics when used as hybrid electrode materials for energy storage applications. From the chemical viewpoint, such a markedly different properties are due to the mixture of imine/phenol and ß-ketoenamine tautomeric forms coexisting in POCOF-1 whereas only the imine-type linkage can be found in POCOF-2. Electrodes composed of POCOF-1 showed a superior electrochemical performance compared to those of POCOF-2 in terms of specific capacitance (125 vs. 84 F/g), areal capacitance (248 vs 170 mF/cm^2) and volumetric capacitance (41.9 vs. 28.6 mF/cm^3), all at a current density of 0.5 A/g, along with a maximum energy density (56.2 vs 38.2 Wh/kg), and maximum power density (3.7 vs 3.6 kW/kg) and greater cyclability (capacitance retention 90 % vs 74 % after 5000 cycles). The enhanced performance of POCOF-1 electrodes

is a result of their large surface area (347 vs 176 m^2/g of POCOF-2), the electrochemical activity of the phenol/keto groups, as well as the higher chemical stability of the ß-ketoenamine form. We foresee that POCOFs with pure ß-ketoenamine form will exhibit an outstanding cycling lifetime due to their high chemical stability. Noteworthy, this is the first keto-enol equilibrium shown in a POM hybrids, which results in an enhanced chemical stability and in a superior electrochemical performance of the POCOF-1 electrodes, when compared with POCOF-2 electrodes that possesses only imine-type linkage and pristine POMs electrodes. Overall, this work paves the way for the rational design of other hybrid COFs based on polyoxometalates, for instance via the modification of the POCOF topology or the center d-block cation of Anderson POM, to be used as high-performing electrodes in energy-related applications.

Acknowledgements

This work was supported by the National Science Centre, Poland (grant no. 2020/36/C/ST5/00247 and UMO-2020/39/D/ST4/01182) and IDUB-AMU programme "50x50: fifty grants for 50 young scientists—038/04/NŚ/0040" as well as the the Agence Nationale de la Recherche through the Interdisciplinary Thematic Institute SysChem via the IdEx Unistra (ANR-10-IDEX-0002) within the program Investissement d'Avenir, the International Center for Frontier Research in Chemistry (icFRC), and the Institut Universitaire de France (IUF).

Conflict of Interest

The authors declare no conflict of interest.

Data Availability Statement

The data that support the findings of this study are available from the corresponding author upon reasonable request.

Keywords: Covalent Organic Framework · Energy Storage Devices · Functional Porous Materials · Hybrid Materials · Polyoxometalate

[1] a) M. De Rosa, O. Afanaseva, A. V. Fedyukhin, V. Bianco, *J. Energy Storage* **2021**, *44*, 103443; b) B. Wang, T. Ruan, Y. Chen, F. Jin, L. Peng, Y. Zhou, D. Wang, S. Dou, *Energy Storage Mater.* **2020**, *24*, 22; c) P. G. Bruce, B. Scrosati, J. M. Tarascon, *Angew. Chem. Int. Ed.* **2008**, *47*, 2930; d) F. Bonaccorso, L. Colombo, G. Yu, M. Stoller, V. Tozzini, A. C. Ferrari, R. S. Ruoff, V. Pellegrini, *Science* **2015**, *347*, 1246501.

[2] a) Z. Yu, L. Tetard, L. Zhai, J. Thomas, *Energy Environ. Sci.* **2015**, *8*, 702; b) A. González, E. Goikolea, J. A. Barrena, R. Mysyk, *Renewable Sustainable Energy Rev.* **2016**, *58*, 1189; c) J. Zhao, A. F. Burke, *J. Energy Chem.* **2021**, *59*, 276; d) J. R. Miller, A. Burke, *Electrochem. Soc. Interface* **2008**, *17*, 53; e) P. Simon, Y. Gogotsi, *Acc. Chem. Res.* **2013**, *46*, 1094.

[3] J. Liu, Z. Bao, Y. Cui, E. J. Dufek, J. B. Goodenough, P. Khalifah, Q. Li, B. Y. Liaw, P. Liu, A. Manthiram, Y. S. Meng, V. R. Subramanian, M. F. Toney, V. V. Viswanathan, M. S. Whittingham, J. Xiao, W. Xu, J. Yang, X.-Q. Yang, J.-G. Zhang, *Nat. Energy* **2019**, *4*, 180.

[4] a) A. Noori, M. F. El-Kady, M. S. Rahmanifar, R. B. Kaner, M. F. Mousavi, *Chem. Soc. Rev.* **2019**, *48*, 1272; b) N. Yang, S. Yu, W. Zhang, H. M. Cheng, P. Simon, X. Jiang, *Adv. Mater.* **2022**, *34*, 2202380;c) M. Pershaanaa, S. Bashir, S. Ramesh, K. Ramesh, *J. Energy Storage* **2022**, *50*, 104599.

[5] H. R. Ghenaatian, M. F. Mousavi, M. S. Rahmanifar, *Synth. Met.* **2011**, *161*, 2017.

[6] J. Yan, Q. Wang, T. Wei, Z. Fan, *Adv. Energy Mater.* **2014**, *4*, 1300816.

[7] a) Y. Jiang, J. Liu, *Energy Environ. Mater.* **2019**, *2*, 30; b) T. S. Mathis, N. Kurra, X. Wang, D. Pinto, P. Simon, Y. Gogotsi, *Adv. Energy Mater.* **2019**, *9*, 1902007.

[8] a) N. I. Gumerova, A. Rompel, *Nat. Chem. Rev.* **2018**, *2*, 0112; b) D.-L. Long, R. Tsunashima, L. Cronin, *Angew. Chem. Int. Ed.* **2010**, *49*, 1736.

[9] A. V. Anyushin, A. Kondinski, T. N. Parac-Vogt, *Chem. Soc. Rev.* **2020**, *49*, 382.

[10] J. J. Walsh, A. M. Bond, R. J. Forster, T. E. Keyes, *Coord. Chem. Rev.* **2016**, *306*, 217.

[11] S. Shigeta, S. Mori, T. Yamase, N. Yamamoto, N. Yamamoto, *Biomed. Pharmacother.* **2006**, *60*, 211.

[12] a) Y. Zhang, J. Liu, S.-L. Li, Z.-M. Su, Y.-Q. Lan, *EnergyChem* **2019**, *1*, 100021; b) S. Yang, M. Wang, Y. Zhang, P. He, W. Cong, C. Wang, Q. Yang, X. Liu, T. Wang, X. Zhang, J. Zhou, *Energy Environ. Mater.* n/*a*.

[13] a) T. Wei, M. Zhang, P. Wu, Y.-J. Tang, S.-L. Li, F.-C. Shen, X.-L. Wang, X.-P. Zhou, Y.-Q. Lan, *Nano Energy* **2017**, *34*, 205; b) M. Zhang, A. M. Zhang, X.-X. Wang, Q. Huang, X. Zhu, X.-L. Wang, L.-Z. Dong, S.-L. Li, Y.-Q. Lan, *J. Mater. Chem. A* **2018**, *6*, 8735; c) D. Kumar, A. Joshi, G. Singh, R. K. Sharma, *Chem. Eng. J.* **2022**, *431*, 134085.

[14] a) Y. Hou, D. Chai, B. Li, H. Pang, H. Ma, X. Wang, L. Tan, *ACS Appl. Mater. Interfaces* **2019**, *11*, 20845; b) P. Yang, J. Xie, L. Wang, X. Chen, F. Wu, Y. Huang, *Adv. Mater. Interfaces* **2020**, *7*, 2000949.

[15] a) A. E. Baumann, D. A. Burns, B. Liu, V. S. Thoi, *Commun. Chem.* **2019**, *2*, 86; b) *Chem. Rev.* **2012**, *112*, 673.

[16] K. Geng, T. He, R. Liu, S. Dalapati, K. T. Tan, Z. Li, S. Tao, Y. Gong, Q. Jiang, D. Jiang, *Chem. Rev.* **2020**, *120*, 8814.

[17] a) X.-X. Li, D. Zhao, S.-T. Zheng, *Coord. Chem. Rev.* **2019**, *397*, 220; b) J. Liu, M. Huang, Z. Hua, Y. Dong, Z. Feng, T. Sun, C. Chen, *ChemistrySelect* **2022**, *7*, e202200546.

[18] Z. H. Wang, X. F. Wang, Z. Tan, X. Z. Song, *Mater. Today Energy* **2021**, *19*, 100618.

[19] a) W. Xu, X. Pei, C. S. Diercks, H. Lyu, Z. Ji, O. M. Yaghi, *J. Am. Chem. Soc.* **2019**, *141*, 17522; b) R. Ma, N. Liu, T.-T. Lin, T. Zhao, S.-L. Huang, G.-Y. Yang, *J. Mater. Chem. A* **2020**, *8*, 8548; c) Y. Zhao, Z. Wang, J. Gao, Z. Zhao, X. Li, T. Wang, P. Cheng, S. Ma, Y. Chen, Z. Zhang, *Nanoscale* **2020**, *12*, 21218; d) M. Lu, M. Zhang, J. Liu, T.-Y. Yu, J.-N. Chang, L.-J. Shang, S.-L. Li, Y.-Q. Lan, *J. Am. Chem. Soc.* **2022**, *144*, 1861; e) X. Yu, C. Li, Y. Ma, D. Li, H. Li, X. Guan, Y. Yan, V. Valtchev, S. Qiu, Q. Fang, *Microporous Mesoporous Mater.* **2020**, *299*, 110105.

[20] S. Kandambeth, A. Mallick, B. Lukose, M. V. Mane, T. Heine, R. Banerjee, *J. Am. Chem. Soc.* **2012**, *134*, 19524.

[21] A. Blazevic, A. Rompel, *Coord. Chem. Rev.* **2016**, *307*, 42.

[22] S. Schönweiz, M. Heiland, M. Anjass, T. Jacob, S. Rau, C. Streb, *Chem. Eur. J.* **2017**, *23*, 15370.

[23] a) R. W. Layer, *Chem. Rev.* **1963**, *63*, 489; b) N. I. Gumerova, A. Rompel, *Chem. Soc. Rev.* **2020**, *49*, 7568.

[24] J. H. Chong, M. Sauer, B. O. Patrick, M. J. MacLachlan, *Org. Lett.* **2003**, *5*, 3823.
[25] C. R. DeBlase, K. E. Silberstein, T.-T. Truong, H. D. Abruña, W. R. Dichtel, *J. Am. Chem. Soc.* **2013**, *135*, 16821.
[26] C. Kang, Z. Zhang, V. Wee, A. K. Usadi, D. C. Calabro, L. S. Baugh, S. Wang, Y. Wang, D. Zhao, *J. Am. Chem. Soc.* **2020**, *142*, 12995.
[27] C. Reichardt, T. Welton, in *Solvents and Solvent Effects in Organic Chemistry*, Wiley-VCH, Weinheim, **2010**, p. 677.
[28] a) J. G. Choi, L. T. Thompson, *Appl. Surf. Sci.* **1996**, *93*, 143; b) J. Chastain, Roger C. King Jr., *Perkin-Elmer Corp.* Handbook of X-ray Photoelectron Spectroscopy, **1992**, *40*.
[29] a) M. C. Daugherty, E. Vitaku, R. L. Li, A. M. Evans, A. D. Chavez, W. R. Dichtel, *Chem. Commun.* **2019**, *55*, 2680; b) R. Wang, W. Kong, T. Zhou, C. Wang, J. Guo, *Chem. Commun.* **2021**, *57*, 331.
[30] L. Yu, G. Z. Chen, *Front. Chem.* **2019**, *7*, 272.
[31] a) M. A. Bhat, *Electrochim. Acta* **2012**, *81*, 275; b) K. H. Hendriks, S. G. Robinson, M. N. Braten, C. S. Sevov, B. A. Helms, M. S. Sigman, S. D. Minteer, M. S. Sanford, *ACS Cent. Sci.* **2018**, *4*, 189; c) P. Navalpotro, J. Palma, M. Anderson, R. Marcilla, *Angew. Chem. Int. Ed.* **2017**, *56*, 12460; d) H. Sheng, A. Zhu, L. Zhang, J. Huang, T. Yang, S. Qin, F. Zhang, Q. Xu, H. Xie, *Green Chem.* **2023**, *25*, 3046.
[32] X. Wu, J. J. Hong, W. Shin, L. Ma, T. Liu, X. Bi, Y. Yuan, Y. Qi, T. W. Surta, W. Huang, J. Neuefeind, T. Wu, P. A. Greaney, J. Lu, X. Ji, *Nat. Energy* **2019**, *4*, 123.
[33] a) J. Shi, B. Jiang, Z. Liu, C. Li, F. Yan, X. Liu, H. Li, ChaoYang, D. Dong, *Ceram. Int.* **2021**, *47*, 18540; b) A. J. Roberts, R. C. T. Slade, *Electrochim. Acta* **2010**, *55*, 7460.
[34] a) G. A. M. Ali, O. A. Habeeb, H. Algarni, K. F. Chong, *J. Mater. Sci.* **2019**, *54*, 683; b) Y. Xu, Z. Lin, X. Huang, Y. Wang, Y. Huang, X. Duan, *Adv. Mater.* **2013**, *25*, 5779.
[35] S. Herrmann, C. Ritchie, C. Streb, *Dalton Trans.* **2015**, *44*, 7092.

Manuscript received: April 14, 2023
Accepted manuscript online: June 19, 2023
Version of record online: June 28, 2023